J|A|C|S ARTICLES

Published on Web 02/02/2010

Interfacial Reactions of Ozone with Surfactant Protein B in a Model Lung Surfactant System

Hugh I. Kim,[†] Hyungjun Kim,[‡,⊥] Young Shik Shin,[§] Luther W. Beegle,[†] Seung Soon Jang,[||] Evan L. Neidholdt,[§] William A. Goddard,[‡] James R. Heath,[§] Isik Kanik,[†] and J. L. Beauchamp*,[§]

Jet Propulsion Laboratory, California Institute of Technology, Pasadena, California 91109, Materials and Process Simulation Center, Beckman Institute, California Institute of Technology, Pasadena, California 91125, Noyes Laboratory of Chemical Physics, California Institute of Technology, Pasadena, California 91125, and School of Materials Science and Engineering, Georgia Institute of Technology, Atlanta, Georgia 30332-0245

Received October 5, 2009; E-mail: jlbchamp@caltech.edu

Abstract: Oxidative stresses from irritants such as hydrogen peroxide and ozone (O_3) can cause dysfunction of the pulmonary surfactant (PS) layer in the human lung, resulting in chronic diseases of the respiratory tract. For identification of structural changes of pulmonary surfactant protein B (SP-B) due to the heterogeneous reaction with O_3, field-induced droplet ionization (FIDI) mass spectrometry has been utilized. FIDI is a soft ionization method in which ions are extracted from the surface of microliter-volume droplets. We report structurally specific oxidative changes of SP-B_{1-25} (a shortened version of human SP-B) at the air−liquid interface. We also present studies of the interfacial oxidation of SP-B_{1-25} in a nonionizable 1-palmitoyl-2-oleoyl-*sn*-glycerol (POG) surfactant layer as a model PS system, where competitive oxidation of the two components is observed. Our results indicate that the heterogeneous reaction of SP-B_{1-25} at the interface is quite different from that in the solution phase. In comparison with the nearly complete homogeneous oxidation of SP-B_{1-25}, only a subset of the amino acids known to react with ozone are oxidized by direct ozonolysis in the hydrophobic interfacial environment, both with and without the lipid surfactant layer. Combining these experimental observations with the results of molecular dynamics simulations provides an improved understanding of the interfacial structure and chemistry of a model lung surfactant system subjected to oxidative stress.

Introduction

The cardiopulmonary system is constantly exposed to airborne environmental hazards. Long-term and immediate exposure of the lungs to pathogens, air pollutants, and other irritants can be a major cause of acute and chronic injuries such as cardiopulmonary mortality and lung cancer.[1−4] Lung disease is the third leading cause of death in the United States; approximately $154 billion is spent for direct and indirect lung-disease-related health care every year.[4] Recently, Jerret et al.[1] studied the effect of tropospheric ozone on the risk of death from any cause and cause-specific death in a large cohort of the United States. They reported a significant increase in the risk of death from respiratory causes in association with an increase in ozone (O_3) concentration from air pollution. Lung disease death rates are still increasing, and more efforts to understand the chemical as well as physical characteristics of the lung system are required.

Pulmonary surfactant (PS) is a mixture of lipids and proteins found in the lungs that reduces the surface tension of the alveolar sacs during the breath cycle.[5] Phospholipids form oriented monolayers at the air−liquid interface, achieving a very low surface tension (~0 mN/m)[6,7] to ease the adsorption and spreading of the air−liquid interface in the lung alveolar sacs.[7] Surfactant protein B (SP-B) enhances phospholipid adsorption and spreading from the subphase to the interface,[6,8,9] and inherited deficiencies in SP-B are lethal at birth.[8,10] Despite its vital importance, little is known about the interactions of this protein with phospholipids in the PS. Furthermore, the detailed

[†] Jet Propulsion Laboratory, California Institute of Technology.
[‡] Materials and Process Simulation Center, Beckman Institute, California Institute of Technology.
[§] Noyes Laboratory of Chemical Physics, California Institute of Technology.
[||] Georgia Institute of Technology.
[⊥] Current Address: Graduate School of EEWS, Korea Advanced Institute of Science and Technology, Daejeon 305-701, Republic of Korea.

(1) Jerrett, M.; Burnett, R. T.; Pope, C. A.; Ito, K.; Thurston, G.; Krewski, D.; Shi, Y. L.; Calle, E.; Thun, M. *N. Engl. J. Med.* **2009**, *360*, 1085–1095.
(2) Anseth, J.; Goffin, A.; Fuller, G.; Ghio, A.; Kao, P.; Upadhyay, D. *Am. J. Respir. Cell Mol. Biol.* **2005**, *33*, 161–168.
(3) Halliwell, B.; Gutteridge, J. *Biochem. J.* **1984**, *219*, 1–14.
(4) Stansfield, A.; Jump, Z.; Sodlosky, S.; Rappaport, S.; Edelman, N.; Haldorsen, J.; Javed, T.; Martin, C.; Margulies, E. *Lung Disease Data: 2008*; American Lung Association: New York, 2008.
(5) Vangolde, L.; Batenburg, J.; Robertson, B. *Physiol. Rev.* **1988**, *68*, 374–455.
(6) Schram, V.; Hall, S. *Biophys. J.* **2004**, *86*, 3734–3743.
(7) Hawco, M.; Davis, P.; Keough, K. *J. Appl. Physiol.* **1981**, *51*, 509–515.
(8) Perez-Gil, J.; Keough, K. *Biochim. Biophys. Acta* **1998**, *1408*, 203–217.
(9) Longo, M. L.; Bisagno, A. M.; Zasadzinski, J. A. N.; Bruni, R.; Waring, A. J. *Science* **1993**, *261*, 453–456.
(10) Clark, J.; Wert, S.; Bachurski, C.; Stahlman, M.; Stripp, B.; Weaver, T.; Whitsett, J. *Proc. Natl. Acad. Sci. U.S.A.* **1995**, *92*, 7794–7798.

10.1021/ja908477w

chemical change of major components when the PS is exposed to oxidants such as O_3 has not been studied thoroughly.

A number of studies have reported chemical changes in major components of the PS under various oxidative stresses,[11−13] as well as changes in physical properties, which cause acute lung injury and respiratory failure.[2,14,15] For example, Uppu et al.[12] used human red-blood-cell membranes as a model lung system and demonstrated their oxidation via a solution-phase O_3 application. However, understanding detailed mechanisms of chemical and physical changes of the PS system at the air−liquid interface is still an active and challenging field of research. In particular, oxidative changes in major PS components by a heterogeneous air−liquid reaction with an external oxidative source (i.e., O_3) have not been studied thoroughly at the molecular level. Air−liquid heterogeneous chemistry of atmospherically relevant molecules has been studied thoroughly using mass spectrometric,[16−18] spectroscopic,[19−22] and surface tensiometric techniques[23,24] along with theoretical methods.[25,26] Fewer studies have considered the air−liquid interfacial chemistry of biologically relevant systems. Exemplifying the latter, Colussi and co-workers recently reported heterogeneous reactions with O_3 of ascorbic acid[27] and uric acid,[28] which are components of the pulmonary epithelial lining fluid, using mass spectrometry.

Field-induced droplet ionization mass spectrometry (FIDI-MS) is a soft ionization method for sampling ions from the surface of microliter droplets.[16,29,30] A pulsed electric field stretches neutral droplets until they develop dual Taylor cones, emitting streams of positively and negatively charged submicrometer droplets in opposite directions. A quiescent hanging droplet is formed on the end of a capillary and then exposed to gas-phase reactants for a variable period of time, after which FIDI-MS sampling of molecular species present in the interfacial layer is performed (Figure 1).

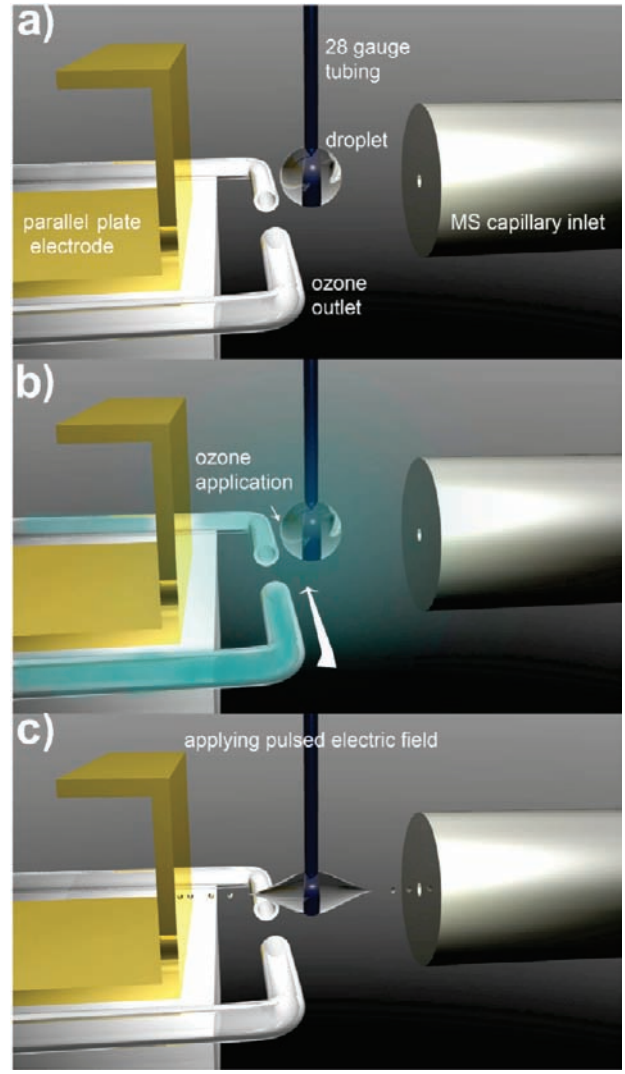

Figure 1. Schematic illustration of the FIDI-MS methodology for studies of interfacial chemistry. (a) A quiescent hanging droplet of analyte-containing solution is formed on the end of a capillary. All of the electrical components remain at ground as the droplet grows and reacts in a field-free environment. (b) The droplet is exposed to gas-phase reactants for a variable period of time, during which heterogeneous reactions occur between the gas-phase and solution-phase species. (c) After a suitable period of reaction, a pulsed electric field stretches the neutral droplet until it emits streams of positively and negatively charged submicrometer droplets in opposite directions. Ionic species present in the interfacial region are sampled though the capillary inlet of the mass analyzer.

In this study, we utilized FIDI-MS to probe air−liquid interfacial oxidation of SP-B_{1-25} (FPIPLPYCWLCRALIKRIQAMI-PKG) by O_3. SP-B_{1-25}, comprising the 25 N-terminal amino acids of wild-type SP-B, mimics the lung activities of the full-length protein.[9,31,32] The structural features of SP-B_{1-25} include predominant α-helical structure (residues 8−22), N-terminal (residues 1−6) β-sheet conformation, and C-terminal (residues 23−25) random structure.[33] We sampled the droplet containing

(11) Pryor, W.; Das, B.; Church, D. *Chem. Res. Toxicol.* **1991**, *4*, 341–348.
(12) Uppu, R. M.; Cueto, R.; Squadrito, G. L.; Pryor, W. A. *Arch. Biochem. Biophys.* **1995**, *319*, 257–266.
(13) Manzanares, D.; Rodriguez-Capote, K.; Liu, S. Y.; Haines, T.; Ramos, Y.; Zhao, L.; Doherty-Kirby, A.; Lajoie, G.; Possmayer, F. *Biochemistry* **2007**, *46*, 5604–5615.
(14) Andersson, S.; Kheiter, A.; Merritt, T. A. *Lung* **1999**, *177*, 179–189.
(15) Rodriguez-Capote, K.; Manzanares, D.; Haines, T.; Possmayer, F. *Biophys. J.* **2006**, *90*, 2808–2821.
(16) Grimm, R. L.; Hodyss, R.; Beauchamp, J. L. *Anal. Chem.* **2006**, *78*, 3800–3806.
(17) Thornberry, T.; Abbatt, J. P. D. *Phys. Chem. Chem. Phys.* **2004**, *6*, 84–93.
(18) Enami, S.; Vecitis, C. D.; Cheng, J.; Hoffmann, M. R.; Colussi, A. J. *Chem. Phys. Lett.* **2008**, *455*, 316–320.
(19) Davis, E. J.; Aardahl, C. L.; Widmann, J. F. *J. Dispersion Sci. Technol.* **1998**, *19*, 293–309.
(20) Buehler, M. F.; Davis, E. J. *Colloids Surf., A* **1993**, *79*, 137–149.
(21) Voss, L. F.; Hadad, C. M.; Allen, H. C. *J. Phys. Chem. B* **2006**, *110*, 19487–19490.
(22) Van Loon, L. L.; Allen, H. C. *J. Phys. Chem. A* **2008**, *112*, 7873–7880.
(23) Gonzalez-Labrada, E.; Schmidt, R.; DeWolf, C. E. *Chem. Commun.* **2006**, 2471–2473.
(24) Gonzalez-Labrada, E.; Schmidt, R.; DeWolf, C. E. *Phys. Chem. Chem. Phys.* **2007**, *9*, 5814–5821.
(25) Mundy, C. J.; Kuo, I. F. W. *Chem. Rev.* **2006**, *106*, 1282–1304.
(26) Chang, T. M.; Dang, L. X. *Chem. Rev.* **2006**, *106*, 1305–1322.
(27) Enami, S.; Hoffmann, M. R.; Colussi, A. J. *Proc. Natl. Acad. Sci. U.S.A.* **2008**, *105*, 7365–7369.
(28) Enami, S.; Hoffmann, M. R.; Colussi, A. J. *J. Phys. Chem. B* **2008**, *112*, 4153–4156.
(29) Grimm, R. L.; Beauchamp, J. L. *J. Phys. Chem. B* **2003**, *107*, 14161–14163.
(30) Grimm, R. L.; Beauchamp, J. L. *J. Phys. Chem. B* **2005**, *109*, 8244–8250.
(31) Takamoto, D. Y.; Lipp, M. M.; von Nahmen, A.; Lee, K. Y. C.; Waring, A. J.; Zasadzinski, J. A. *Biophys. J.* **2001**, *81*, 153–169.
(32) Bruni, R.; Taeusch, H. W.; Waring, A. J. *Proc. Natl. Acad. Sci. U.S.A.* **1991**, *88*, 7451–7455.
(33) Gordon, L. M.; Lee, K. Y. C.; Lipp, M. M.; Zasadzinski, J. A.; Walther, F. J.; Sherman, M. A.; Waring, A. J. *J. Pept. Res.* **2000**, *55*, 330–347.

Scheme 1. Structures of POG and SP-B_{1-25} Investigated in This Study

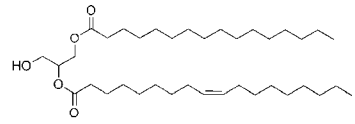

1-Palmitoyl-2-oleoyl-*sn*-glycerol (POG)

Phe_1-Pro_2-Ile_3-Pro_4-Leu_5-Pro_6-Tyr_7-Cys_8-Trp_9-Leu_{10}-Cys_{11}-Arg_{12}-Ala_{13}-Leu_{14}
Gly_{25}-Lys_{24}-Pro_{23}-$Ileu_{22}$-Met_{21}-Ala_{20}-Gln_{19}-Ile_{18}-Arg_{17}-Lys_{16}-Ile_{15}

SP-B_{1-25}

SP-B_{1-25} exposed to a constant flux of O_3 gas over a range of reaction times to analyze distinct air−liquid interfacial chemistry. Next, we investigated the difference between the interfacial and solution-phase reactions of O_3 with SP-B_{1-25}. Oxidation using the Fenton reaction was also performed to compare the solution-phase ozonolysis to solution-phase oxidation by OH radical. Finally, we investigated the heterogeneous reaction of a model PS system composed of SP-B_{1-25} and 1-palmitoyl-2-oleoyl-*sn*-glycerol (POG) with O_3. POG is nonionizable lipid that was used in order to avoid undesired competition of ionization with SP-B_{1-25} at the surface of the droplet during the FIDI experiment. The structures of POG and SP-B_{1-25} are shown in Scheme 1. To more fully interpret the experimental observations, the positioning of SP-B_{1-25} in a lipid monolayer was examined using molecular dynamics (MD) simulations.

Experimental and Computational Methods

Chemicals and Reagents. Ammonium bicarbonate (NH_4HCO_3), iron(II) dichloride ($FeCl_2$), sodium ethylenediaminetetraacetic acid (EDTA), and trypsin from porcine pancreas were purchased from Sigma-Aldrich (St. Louis, MO). SP-B_{1-25} was purchased from Biomer Technology (Hayward, CA). Sodium salts of POG were purchased from Avanti Polar Lipids (Alabaster, AL). All of the solvents (hydrogen peroxide, water, methanol, and acetic acid) were purchased from EMD Chemicals Inc. (Gibbstown, NJ).

Online FIDI-MS Technique and Heterogeneous Oxidation by O_3. The FIDI-MS instrument used in this investigation was based on designs previously described by Grimm et al.[16] A droplet (∼2 mm o.d.) of analyte solution was suspended from the end of a 28 gauge stainless steel capillary (Small Parts Inc.), which was located between the atmospheric sampling inlet of a Thermo Finnigan LCQ Deca mass spectrometer and a parallel-plate electrode. The droplet was located on center in the region between the plate electrode and the mass spectrometer inlet; the plate and inlet were separated by 6 mm. The O_3 outlet was located 1 mm from the droplet in order to reduce mechanical perturbation of the droplet by the flow of O_3. Ozonolysis reactions occurred between 0 and 30 s after a quiescent droplet was achieved (1−2 s). Next, a high-voltage pulse was applied on the parallel plate electrode and sampling capillary. The high-voltage pulse established a field of $\pm 7 \times 10^5$ V m^{-1} with a 20 ms duration to achieve FIDI. This is just above the threshold required for FIDI to be observed. A pencil-style UV calibration lamp (model 6035, Oriel) generated ∼20 ppm O_3 (measured spectrophotometrically using an absorption cell with a 10 cm path length and calculated with Beer's law using a molar absorption coefficient of 1.15×10^{-17} cm^2 $molecule^{-1}$) in air that continually washed through the FIDI region at 1500 mL min^{-1}. Because of its high toxicity, the ozone level in the laboratory was monitored using ozone test strips (OzoneLab, Canada), and all of the experimentalists used particulate filter masks (3M, St. Paul, MN) for personal protection during the experiment. Either 50 μM SP-B_{1-25} or a mixture of 100 μM POG and 50 μM SP-B_{1-25} in 1:1 (v/v) water/methanol fed the droplet source. A previous study of the secondary structure of SP-B_{1-25} reported that the peptide conserves its predominate α-helical conformation in aqueous, lipid, and alcohol environments.[33] We assumed that the peptide preserves its α-helical structure in either a water/methanol mixture or a POG monolayer. Negative or positive 4 and 2 kV, 20 ms pulses to the plate electrode and capillary, respectively, were used to initiate FIDI and direct charged progeny into the LCQ for mass analysis in positive (SP-B_{1-25}) mode. The FIDI-MS spectra reported in this study were obtained by averaging 5−10 individually acquired spectra from separately prepared droplets. The nomenclature proposed by Roepstorff and Fohlman[34] is used for the parent and fragment ions.

Solution-Phase O_3 Reaction. A continuous flow of ∼20 ppm O_3 in air was applied to the 100 μM SP-B_{1-25} solution in 1:1 (v/v) water/methanol solvent for 30 s and 1, 1.5, 2, 3, 4, and 5 min. The SP-B_{1-25} solution was diluted to 50 μM for electrospray ionization (ESI) with 1:1 (v/v) water/methanol containing 1% acetic acid by volume. Product analysis was performed on a Micromass QTof2 quadrupole time-of-flight mass spectrometer in the positive-ion mode. Trypsin digests of SP-B_{1-25} and O_3-treated SP-B_{1-25} were prepared by incubating 200 μM SP-B_{1-25} with 6 μg of trypsin from porcine pancreas in 1 mL of water containing 25 mM ammonium bicarbonate (NH_4HCO_3) at 37 °C for 4 h. The trypsin was then removed using a Millipore Microcon centrifugal filter fitted with an Ultracel YM-10 membrane. The sample solution was diluted to an appropriate concentration for ESI with 1:1 (v/v) water/methanol containing 1% acetic acid by volume. Product analysis was performed on a Thermo Finnigan LCQ Deca XP ion trap mass spectrometer (ITMS) in positive and negative modes.

Fenton Reaction. SP-B_{1-25} (500 μM) was incubated with 600 μM $FeCl_2$, 600 μM sodium EDTA, and 30 mM H_2O_2 in 1 mL of water at 37 °C for 12, 18, and 24 h. The peptide was purified using a Varian C_{18} OMIX 100 μL pipet tip. The sample solution was diluted to an appropriate concentration with 1:1 (v/v) water/methanol containing 1% acetic acid by volume. Product analysis was performed on a Micromass QTof2 quadrupole time-of-flight mass spectrometer in the positive-ion mode.

Molecular Dynamics Simulations. The MD simulations were performed with the all-atom CHARMM PARAM27[35] force field using the Large-scale Atomic/Molecular Massively Parallel Simulator (LAMMPS) code.[36] To describe the water, we used a flexible TIP3P potential, which needed the additional Hooke's constants $k = 900$ kcal mol^{-1} $Å^{-2}$ for the OH bond and $k = 110$ kcal mol^{-1} rad^{-2} for the H−O−H angle in the three-site-rigid TIP3P model.[35] The initial conformation of SP-B_{1-25} was taken from the Protein Data Bank structure (PDB entry 1DFW). The particle−particle particle-mesh method[37] was employed to compute the electrostatic interactions using an accuracy criterion of 10^{-4}.

The initial structures for the lipid monolayer−water systems were prepared with 48 hexagonally packed lipids on 3168, 3264, 3744, and 4464 water molecules for the 55, 60, 65, and 70 $Å^2$/lipid surface densities, respectively. The purely repulsive wall potential $E = \varepsilon[^2/_{15}(\sigma/r)^9 - (\sigma/r)^3]$, with $\varepsilon = 0.1521$ kcal/mol, $\sigma = 3.1538$ Å, and a cutoff distance of 2.7071 Å, was applied at $z = 0$ to prevent the water from diffusing in the negative z direction. The dimensions of the simulation cells used were (55.21 Å × 47.82 Å × 200.0 Å) for the 55 $Å^2$/lipid, (57.67 Å × 49.94 Å × 200.0 Å) for the 60 $Å^2$/lipid, (60.02 Å × 51.98 Å × 200.0 Å), for the 65 $Å^2$/lipid, and (62.28 Å × 53.94 Å × 200.0 Å) for the 70 $Å^2$/lipid surface densities. The systems were equilibrated for 0.5 ns using 300 K *NVT* MD simulations by applying a Nose−Hoover thermostat with a temperature damping relaxation time of 0.1 ps. Next, 2.0 ns *NVT*

(34) Roepstorff, P.; Fohlman, J. *Biomed. Mass Spectrom.* **1984**, *11*, 601–601.
(35) MacKerell, A. D.; et al. *J. Phys. Chem. B* **1998**, *102*, 3586–3616.
(36) Plimpton, S. *J. Comput. Phys.* **1995**, *117*, 1–19.
(37) Hockney, R. W.; Eastwood, J. W. *Computer Simulation Using Particles*; McGraw-Hill: New York, 1981.

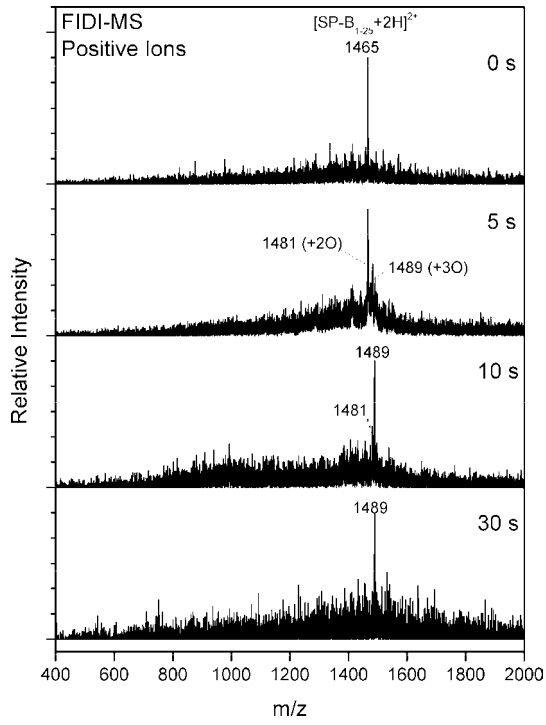

Figure 2. Air−liquid interfacial oxidation of SP-B_{1-25} by O_3 as a function of time. In the absence of ozone, the positive-ion FIDI-MS spectrum of SP-B_{1-25} is dominated by the doubly protonated SP-B_{1-25} peak at *m*/*z* 1465. The products at *m*/*z* 1481 and 1489, corresponding to doubly protonated SP-B_{1-25} with two and three oxygen atoms, respectively, appear after the droplet is exposed to O_3 for 5 s. The triply oxygenated product at *m*/*z* 1489 dominates the FIDI-MS spectrum after exposure of the droplet to O_3 for 10 s. No further oxidation of the peptide is observed up to 30 s of exposure.

MD simulations were performed, and these trajectories were employed for the analysis of the atomic profiles.

The initial structure for the SP-B_{1-25} in the POG or 1-palmitoyl-2-oleoyl-phosphatidylglycerol (POPG) monolayer was constructed using the final structure after the simulation of the lipid monolayer−water system with a surface density of 60 Å^2. After removal of six neighboring lipids, the SP-B_{1-25} was inserted into the resultant cavity with an α-helical axis orientation angle of 34° with respect to the interfacial plane. The dimensions of the simulation cells then were slightly adjusted to (57.88 Å × 50.12 Å × 200.0 Å). Similar to the lipid monolayer simulations, a 0.5 ns equilibration followed by a 2.0 ns *NVT* MD simulation was performed at 300 K. To analyze the trajectories, we averaged the population over the last 0.5 ns of the 2.0 ns trajectories. In order to consider effects of only the waters near the interface, the oxygen atoms with $\Delta z > -15$ Å were included in analyzing the *xy*-projected populations of the water.

Results and Discussion

Interfacial Oxidation of SP-B_{1-25}. The positive-ion FIDI-MS spectrum of SP-B_{1-25} is shown in the top panel of Figure 2. The doubly protonated SP-B_{1-25} is observed as the dominant species in the FIDI-MS spectrum before O_3 application. As discussed earlier, FIDI-MS samples ions from the surface of the droplet.[16] SP-B_{1-25} contains four cationic amino acid (AA) residues, which are Arg_{12}, Lys_{16}, Arg_{17}, and Lys_{24} (Scheme 1). The peptide exhibits amphiphilic characteristics with a hydrophobic N-terminal side and a hydrophilic C-terminal side. The hydrophobic N-terminal side of the peptide is expected to project above the air−liquid interface, while the hydrophilic C-terminal side remains solvated at the interface. In contrast to the other strongly basic AA residues, Arg_{12} is located between Leu_{10} and Leu_{14} in the hydrophobic portion of the peptide (Scheme 1). We suggest that the observed doubly charged SP-B_{1-25} likely results from protonation of Lys_{24} and Arg_{17} in the solvated hydrophilic portion of the peptide. Protonation of Lys_{16} is not as likely because of coulomb repulsion with the adjacent cationic arginine.

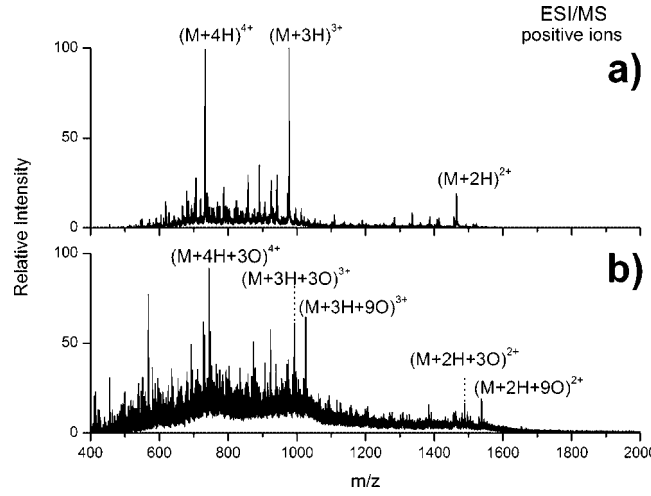

Figure 3. (a) ESI-MS spectrum of SP-B_{1-25}. (b) ESI-MS spectrum of the oxidized products of SP-B_{1-25} after 3 min of solution-phase O_3 reaction.

The time-resolved oxidation of SP-B_{1-25} by O_3 was monitored using FIDI-MS (Figure 2). Products resulting from the oxidation of SP-B_{1-25} by O_3 appear after the droplet is exposed to O_3 for 5 s. The products at *m*/*z* 1481 and 1489 correspond to doubly protonated SP-B_{1-25} with two and three oxygen atoms, respectively. The FIDI-MS spectrum of the droplet with SP-B_{1-25} is dominated by the triply oxygenated product at *m*/*z* 1489 after exposure of the droplet to O_3 for 10 s. No further oxidation of the peptide is observed up to 30 s of exposure. The FIDI-MS spectra imply that the doubly oxygenated product immediately undergoes further oxidation to form the stable product with three oxygen atoms.

Solution-Phase Oxidation of SP-B_{1-25}. In order to investigate the difference between the interfacial and solution-phase reactions of O_3 with SP-B_{1-25}, O_3 was bubbled into a solution containing SP-B_{1-25}. Oxidation using the Fenton reaction was also performed to compare the solution-phase ozonolysis to solution-phase oxidation by OH radical. For the comparison to heterogeneous ozonolysis of SP-B_{1-25}, the products with three additional oxygen atoms from both reactions were analyzed.

In contrast to the FIDI-MS spectrum, triply and quadruply protonated SP-B_{1-25} are observed as the dominant ions in the ESI-MS spectrum, with a smaller amount of the doubly protonated peptide (Figure 3a). No significant oxygenated product is observed when O_3 is applied to the peptide solution for 30 s or less. However, after 1 min of O_3 application, incorporation of three and nine oxygens in SP-B_{1-25} are observed as major products. Other less abundant oxygenated peptides (with four and five more O atoms) are also observed as minor products in the spectrum. No further oxidized product is observed after application of O_3 for 5 min. Figure 3b shows oxidized products of SP-B_{1-25} after application of O_3 to the SP-B_{1-25} solution for 3 min, with the predominant threefold- and ninefold-oxygenated SP-B_{1-25} products indicated in the spectrum. The relative abundance of ninefold-oxygenated SP-B_{1-25} with respect to threefold-oxygenated peptide increases as the charge state of the ions decreases. It is suggested that the more

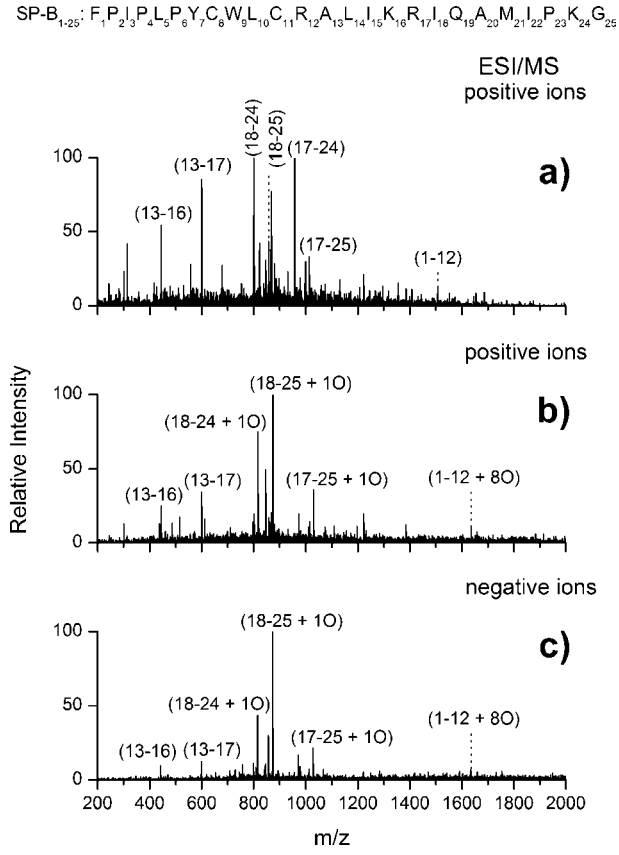

Figure 4. (a) Positive-ion ESI mass spectrum of the trypsin digest of SP-B_{1-25}. (b) Positive-ion ESI mass spectrum of the trypsin digest of the oxidized SP-B_{1-25} from the 3 min solution-phase O_3 reaction. (c) Negative-ion ESI mass spectrum of the trypsin digest of oxidized SP-B_{1-25} from the 3 min solution-phase O_3 reaction.

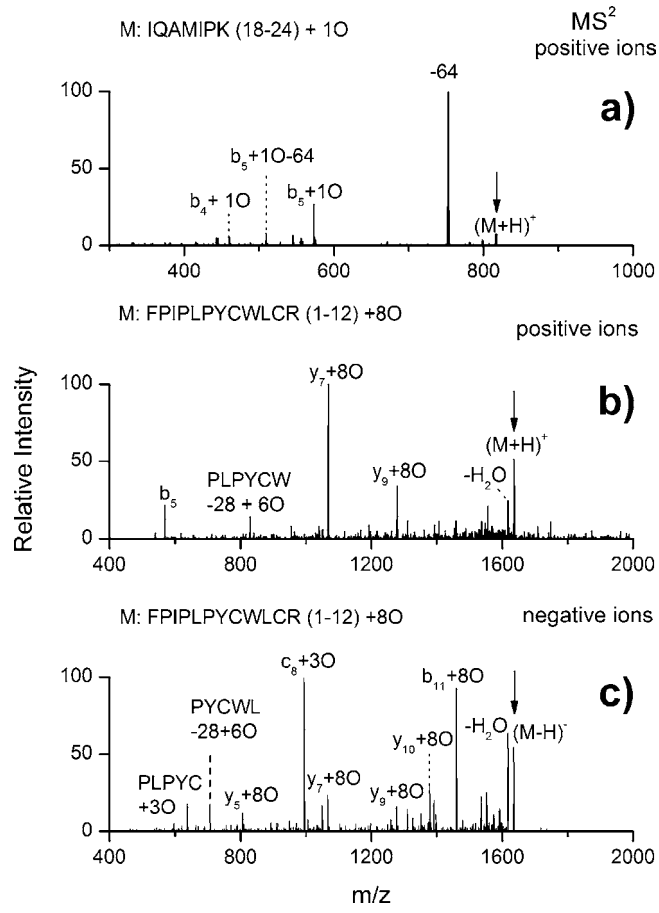

Figure 5. CID spectra of (a) cationic IQAMIPK + 3O at *m*/*z* 817 from the tryptic digest of oxidized SP-B_{1-25}, (b) cationic FPIPLPYCWLCR + 8O at *m*/*z* 1636 from the tryptic digest of oxidized SP-B_{1-25}, and (c) anionic FPIPLPYCWLCR + 8O at *m*/*z* 1634 from the tryptic digest of oxidized SP-B_{1-25}.

completely oxidized species does not yield an abundant +4 charge-state ion because oxidized residues such as cysteic acids form salt bridges with basic AA residues (i.e., Arg and Lys) of the peptide. The oxidized products of triply and quadruply charged SP-B_{1-25} from the Fenton reaction with intact SP-B_{1-25} are shown in Figure S1 in Supporting Information. The Fenton reaction yields a series of oxidized SP-B_{1-25} products with up to 10 oxygen atoms.

Structure Analysis of Extensively Oxidized SP-B_{1-25} from Solution-Phase Ozonolysis. In order to determine the structures of the oxidized SP-B_{1-25} formed by the solution-phase O_3 reaction, a trypsin digest was performed after applying O_3 to the SP-B_{1-25} solution for 3 min. The ESI mass spectrum of a trypsin digest of SP-B_{1-25} exhibits seven major ion peaks. The masses and segments of the observed tryptic digest ions of SP-B_{1-25} are indicated in Figure 4a. The positive-ion ESI mass spectrum of a trypsin digest of SP-B_{1-25} oxidized by reaction with solution-phase O_3 exhibits segments with MetSO (*m*/*z* 817, 874, and 1030) and the less abundant N-terminal segment of FPIPLPYCWLCR + 8O at *m*/*z* 1636 (Figure 4b). The negative-ion ESI mass spectrum also exhibits corresponding deprotonated segment ion peaks (Figure 4c).

The structures of the segments were confirmed by collision-induced dissociation (CID) spectra. As shown in Figure 5a, CID of the ion at *m*/*z* 817 exhibits the elimination of hydrosulfinylmethane (CH_4SO, 64 mass units), which is the characteristic dissociation pathway of methionine sulfoxide (MetSO).[38,39] The structure of the segment FPIPLPYCWLCR + 8O was also investigated using CID. CID of cationic FPIPLPYCWLCR + 8O at *m*/*z* 1636 yields y-type fragments (y_7 and y_9) with all eight oxygen atoms as dominant products (Figure 5b). The fragment PLPYCW with six oxygen atoms indicates that Cys_8 and Trp_9 are oxidized to sulfonic acid (+3O) and hydroxy-*N*-formylkynurenine (HNFKyn) (+3O), respectively (Scheme 2). The structures are further confirmed by the fragments of c_8 + 3O and PLPYC + 3O resulting from CID of FPIPLPY-CWLCR + 8O in negative-ion mode (Figure 5c). The two extra oxygen atoms are assigned to Cys_{11} (+2O). It is notable that Cys_8 and Cys_{11} are located in close proximity to each other in the helical structure.[32] The fact that we did not observe formation of sulfonic acid for both of the closely located Cys residues is possibly due to the formation of sulfonic anhydride ($R_1-O_2SOSO_2-R_2$). No significant segment peak is observed from triply oxygenated SP-B_{1-25} after tryptic digest of the products from the solution-phase O_3 reaction.

Comparative Structure Analysis of Triply Oxygenated SP-B_{1-25} from Solution-Phase and Interfacial Ozonolysis. In comparison with the more extensive solution-phase oxidation

(38) Clauser, K. R.; Hall, S. C.; Smith, D. M.; Webb, J. W.; Andrews, L. E.; Tran, H. M.; Epstein, L. B.; Burlingame, A. L. *Proc. Natl. Acad. Sci. U.S.A.* **1995**, *92*, 5072–5076.
(39) Qin, J.; Chait, B. T. *Anal. Chem.* **1997**, *69*, 4002–4009.

Scheme 2. Mechanisms for Oxidation of Trp, Met, and Cys in Peptides by Reactive Oxygen Species

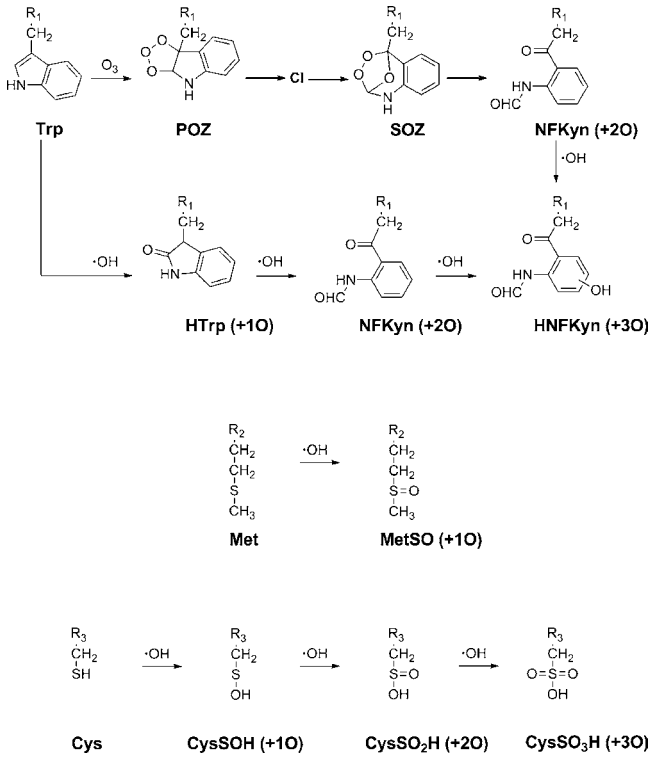

of SP-B_{1-25}, the interfacial reaction results in the addition of only three oxygen atoms to the protein fragment. It is of interest to compare the structures of the triply oxygenated products from the two reactions using CID. The FIDI-CID (FIDI-MS^2) spectrum of the triply oxygenated SP-B_{1-25} product at *m*/*z* 1489 from the heterogeneous oxidation is shown in Figure 6a. CID yields an exclusive fragment at *m*/*z* 1457 resulting from the elimination of CH_4SO. This indicates that the oxidation of the methionine residue (Met_{21}) in SP-B_{1-25} results from the heterogeneous ozonolysis. The other two oxygen atoms are added to the tryptophan residue (Trp_9), forming NFKyn (Scheme 2).

Figure 6b,c shows CID spectra (ESI-MS^2) of the triply oxygenated products of quadruply protonated SP-B_{1-25} from the solution-phase O_3 application and the Fenton reaction, respectively. The ESI-MS^2 spectrum of the triply oxygenated SP-B_{1-25} from the solution-phase O_3 application implies the presence of two products, one with NFKyn (+2O) and MetSO (+1O) and the other with HNFKyn (+3O) (Figure 6b). Evidence of the MetSO in the oxidized SP-B_{1-25} is found from the CID experiment involving the quadruply charged SP-B_{1-25} product from the solution-phase O_3 reaction. For example, the paired $y_{20} - CH_4SO$ and y_{20} fragments, which are respectively observed at *m*/*z* 782 and 803 (triply charged) and at *m*/*z* 1172 and 1204 (doubly charged), confirm the presence of MetSO (Figure 6b). Interesting CID fragments are also observed in the ESI-MS^2 spectrum. The singly charged fragments at *m*/*z* 680, 832, and 938 are WLCRA + 3O, LPYCWLCRALIKR + 3O and PLPYCWLCRALIKRI + 3O, respectively. These fragments are evidence of the formation of HNFKyn through the oxidation of Trp_9 from the solution-phase O_3 reaction. This is further supported by the singly charged QAMIPK $- NH_3$ fragment at *m*/*z* 652, which indicates that no oxidation has occurred at Met_{21}. The ESI-MS^2 spectrum of the triply oxygenated SP-B_{1-25} from the solution-phase O_3 reaction implies the presence of two

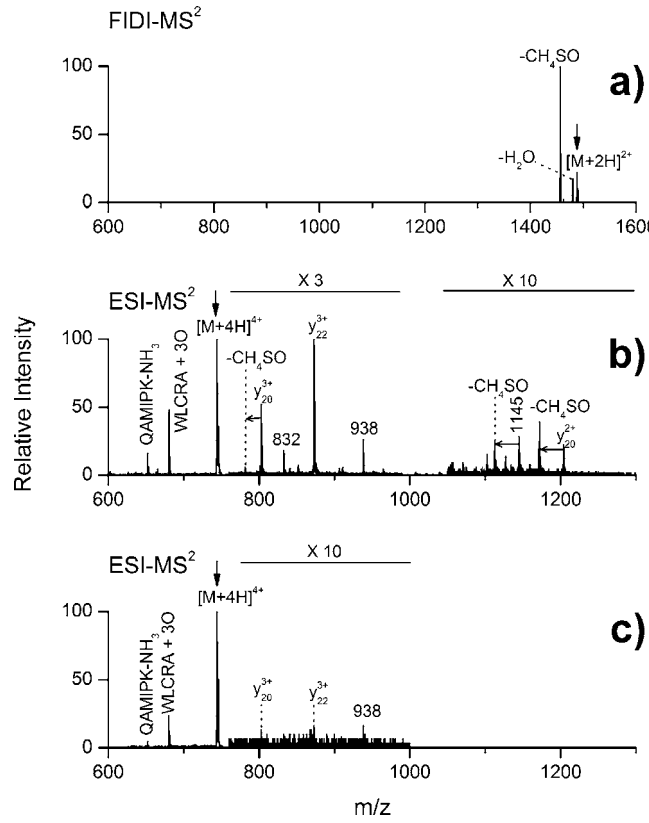

Figure 6. (a) FIDI-MS^2 spectrum of the triply oxygenated products of doubly protonated SP-B_{1-25} from heterogeneous ozonolysis. (b) ESI-MS^2 spectrum of triply oxygenated quadruply protonated SP-B_{1-25} from the solution-phase O_3 reaction. (c) ESI-MS^2 spectrum of triply oxygenated quadruply protonated SP-B_{1-25} from the Fenton reaction. M denotes the parent ion, which is triply oxygenated SP-B_{1-25}.

products, one with NFKyn (+2O) and MetSO (+1O) and the other with HNFKyn (+3O). The CID fragment abundance implies that the solution-phase O_3 reaction with SP-B_{1-25} yields more product peptides with HNFKyn than product peptides with NFKyn and MetSO. The ESI-MS^2 spectrum of the SP-B_{1-25} product from the Fenton reaction is shown in Figure 6c. CID of the Fenton product exhibits the presence of HNFKyn at *m*/*z* 652, 680, and 938, which correspond to the singly charged fragments QAMIPK $- NH_3$, WLCRA + 3O, and PLPYCWLCRALIKRI + 3O, respectively. However, evidence for the formation of the product with NFKyn and MetSO is not found in the spectrum.

Unique Features of the Interfacial Reaction of SP-B_{1-25} with O_3. Ozone has limited solubility in water. For a gas-phase O_3 concentration of 20 ppm, the equilibrium concentration of O_3 dissolved in aqueous solution is calculated to be 22.6 nM using Henry's law.[40] In addition, O_3 is unstable in water and rapidly forms secondary reactive oxygen species (ROS).[41] The major secondary ROS formed by O_3 in water is OH radical.[42] This implies that two major O_3 oxidation pathways, involving ozonolysis and reaction with OH radical, can be observed at the air−liquid interface. The triply oxygenated SP-B_{1-25} is formed concomitantly with the formation of the doubly oxygen-

(40) Seinfeld, J. H.; Pandis, S. N. *Atmospheric Chemistry and Physics: From Air Pollution to Climate Change*; John Wiley & Sons: New York, 1998.
(41) von Gunten, U. *Water Res.* **2003**, *37*, 1443–1467.
(42) Pryor, W. A. *Free Radical Biol. Med.* **1994**, *17*, 451–465.

ated SP-B_{1-25} after exposure of the droplet to O_3 for 5−10 s (Figure 2). The oxidation mechanisms of Trp, Met, and Cys in peptides are shown in Scheme 2. NFKyn can be formed via direct ozonolysis of Trp[43] or hydrolysis of hydroxytryptophan (HTrp).[13] However, the formation of MetSO from Met occurs primarily by secondary oxidants.[44] The NFKyn from the heterogeneous reaction results from the direct ozonolysis of Trp_9, which is located on the hydrophobic N-terminal side of SP-B_{1-25}. Met_{21}, which likely forms MetSO, is located on the hydrophilic C-terminal side. Intact Cys_8 and Cys_{11} support this observed O_3 oxidation of SP-B_{1-25}. The reactivity of Cys with ozone in the solution phase exceeds that of Trp and Met by 2 orders of magnitude.[45] However, the oxidation of Cys to yield cysteinesulfonic acid ($CysSO_3H$) occurs primarily by reactions with secondary oxidants[46] that are formed only in the presence of an aqueous environment. This suggests that the hydrophobic N-terminal side of SP-B_{1-25}, where Cys_8 and Cys_{11} are located, is above the air−liquid interface, while the hydrophilic C-terminal side is immersed in the aqueous layer below the interface. The difference between the solution-phase O_3 application and the heterogeneous ozonolysis is clearly observed from the CID of triply oxygenated SP-B_{1-25} (Figure 6). The formation of HNFkyn requires at least one secondary oxidation step (Scheme 2). After NFKyn is formed by either direct ozonolysis or reaction with secondary oxidants, Met and NFKyn undergo competitive oxidation by secondary ROS in the solution phase to yield MetSO ($k = 1.4 \times 10^{-11}$ cm^3 molecule^{-1} s^{-1}) and HNFKyn ($k = 1.3 \times 10^{-11}$ cm^3 molecule^{-1} s^{-1}).[47]

The observed high abundance of SP-B_{1-25} in which three and nine oxygen atoms have been added from solution-phase ozonolysis can be also explained by the distinct oxidation mechanisms of O_3 in aqueous solution (Figure 3b). The interfacial reactions leading to oxidation of Trp_9 and Met_{21} to form NFKyn and MetSO by ozonolysis and secondary ROS, respectively, render the peptide more hydrophilic. The decrease in the signal-to-noise ratio for the triply oxygenated SP-B_{1-25} in the FIDI-MS spectra with extensive ozonolysis (Figure 2) suggests that this hydrophilic product dissolves in the bulk liquid. This causes NFKyn, Cys_8, and Cys_{11} to be exposed to secondary ROS for further oxidation. As a result, NFKyn reacts with secondary ROS to form HNFKyn, and simultaneously, Cys_8 and Cys_{11} are also oxidized by secondary ROS to form sulfonic anhydride.

Oxidation of SP-B_{1-25} by O_3 in a POG Surfactant Layer. The interfacial reaction of SP-B_{1-25} with ozone was also examined in the presence of the neutral lipid POG, which forms a surfactant layer at the air−liquid interface. FIDI-MS spectra that are almost identical to the spectra obtained for interfacial ozonolysis of SP-B_{1-25} without POG, except for a ∼5 s time delay for initiation of the reaction, are observed (Figure 7). The FIDI-MS spectrum of the SP-B_{1-25}/POG droplet is dominated by the triply oxygenated product after 15 s of exposure. No further oxidation of the peptide is observed up to 30 s exposure. The observed ozonolysis products and time delay of the reaction provide critical clues regarding the location and orientation of SP-B_{1-25} in the monolayer.

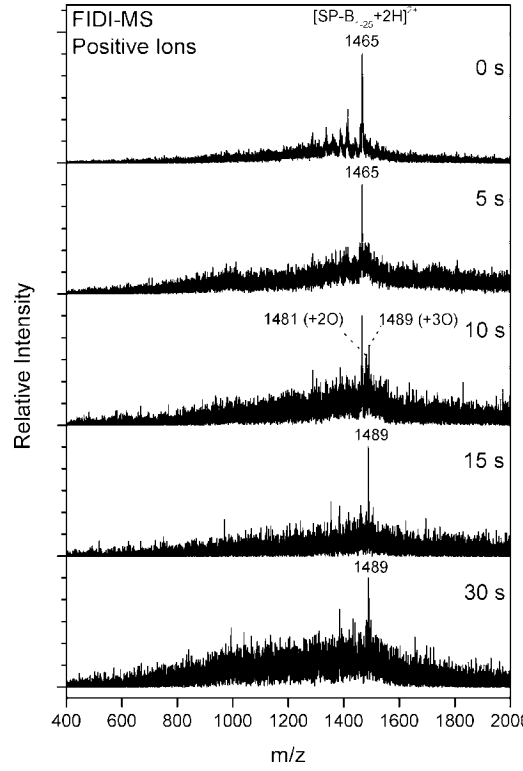

Figure 7. Air−liquid interfacial oxidation of SP-B_{1-25} by O_3 in the POG monolayer as a function of time. Doubly protonated SP-B_{1-25} products with two and three oxygen atoms appear after the droplet is exposed to O_3 for 10 s. The triply oxygenated product dominates the FIDI-MS spectrum after the droplet is exposed to O_3 for 15 s, and no further oxidation of the peptide is observed up to 30 s of exposure.

The kinetics of the heterogeneous ozonolysis of unsaturated phospholipids has been studied previously by several research groups.[24,48,49] Unsaturated phospholipid disappears at the interface by ozonolysis through the formation of a primary ozonide. Under the assumption that the O_3 concentration is constant (∼5×10^{14} molecules cm^{-3}) during the reaction, we can estimate the reaction time using the pseudo-first-order rate constant $k_2 = k_1[O_3]$, where $k_1 = 4.5 \times 10^{-16}$ cm^3 molecule^{-1} s^{-1} [adopted from the 1-oleoyl-2-palmitoyl-*sn*-glycero-3-phosphocholine (OPPC) ozonolysis on NaCl[48]]. The reaction rate is expressed as

$$-\frac{d[POG]_{surf}}{dt} = k_2[POG]_{surf} \quad (1)$$

The time needed to consume 90−99% of the unsaturated lipid to form the primary ozonide and subsequent products at the air−liquid interface is calculated to be 10−20 s. Both POG and OPPC possess a palmitic acid chain and an oleic acid chain, the latter of which reacts with O_3. Under the assumption that the reactivity of POG is similar to that of OPPC, initiation of the SP-B_{1-25} ozonolysis is expected after the droplet is exposed to O_3 for 10−20 s if the peptide is completely shielded by lipid acyl chains. However, the observed short time delay of the initiation of SP-B_{1-25} ozonolysis suggests that the peptide competes directly with POG to react with O_3. This suggests a

(43) Pryor, W. A.; Uppu, R. M. *J. Biol. Chem.* **1993**, *268*, 3120–3126.
(44) Schoneich, C. *Biochem. Biophys. Acta* **2005**, *1703*, 111–119.
(45) Pryor, W. A.; Giamalva, D. H.; Church, D. F. *J. Am. Chem. Soc.* **1984**, *106*, 7094–7100.
(46) Berlett, B. S.; Stadtman, E. R. *J. Biol. Chem.* **1997**, *272*, 20313–20316.
(47) Buxton, G. V.; Greenstock, C. L.; Helman, W. P.; Ross, A. B. *J. Phys. Chem. Ref. Data* **1988**, *17*, 513–886.
(48) Karagulian, F.; Lea, A. S.; Dilbeck, C. W.; Finlayson-Pitts, B. J. *Phys. Chem. Chem. Phys.* **2008**, *10*, 528–541.
(49) Vieceli, J.; Ma, O. L.; Tobias, D. J. *J. Phys. Chem. A* **2004**, *108*, 5806–5814.

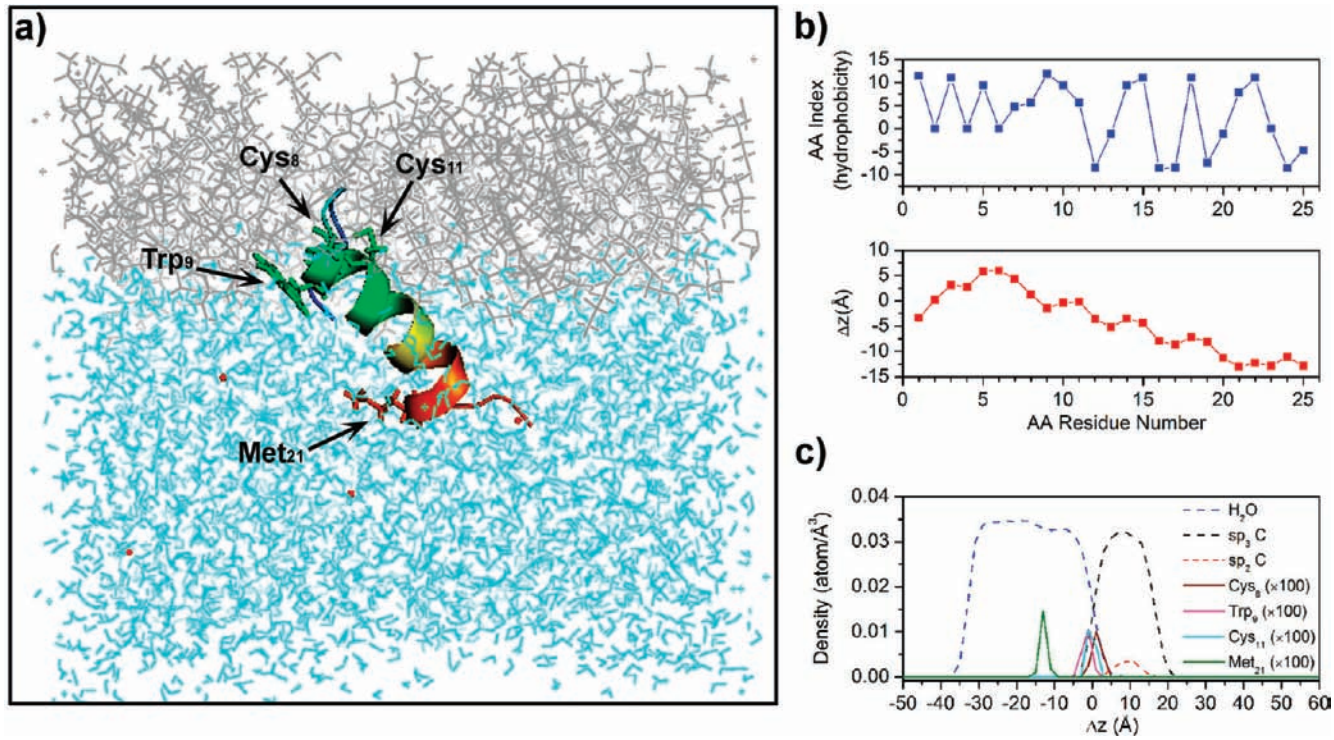

Figure 8. (a) Final snapshot after a 2.0 ns MD simulation of SP-B_{1-25} in a POG monolayer at 60 Å^2/lipid. The peptide is shown in rainbow color (C-terminal, red; N-terminal, blue). Lipids, water molecules, and chlorides are shown in purple, cyan, and red, respectively. (b) AA index for the hydrophobicity scale[53] (top) and Δz for C_α of each residue averaged during the last 0.5 ns of a trajectory of 2.0 ns duration from the MD simulation (bottom) are plotted as functions of amino acid residue number. The air−water interface is located near $\Delta z = 0$. (c) Atomic density profiles of SP-B_{1-25} in a POG monolayer at 60 Å^2/lipid as a function of Δz during the last 0.5 ns of the 2.0 ns MD simulation. The blue dashed line denotes the density profiles of the oxygen atoms of water molecules. Black and red dashed lines denote those of the saturated and unsaturated carbons of lipid acyl chains, respectively. Wine, magenta, cyan, and olive solid lines denote the 100-times-scaled density profiles of the C_α carbons of Cys_8, Trp_9, Cys_{11}, Met_{21} residues, respectively.

picture in which the peptide is colocated with POG at the air−liquid interface at the surface of the droplet. In addition, the ozonolysis of SP-B_{1-25} in the POG monolayer yields products identical to those for the ozonolysis of the peptide alone at the air−liquid interface. This supports the conjecture that SP-B_{1-25} by itself forms an oriented interfacial aggregate or layer at the surface of the droplet. The generally hydrophobic N-terminal portion appears to be packed together in a region depleted of water at the surface of the droplet.

Interactions of SP-B_{1-25} in a Lipid Monolayer. We carried out MD simulations for the POG monolayer in a water box for 2.0 ns with four different surface densities (55, 60, 65, and 70 Å^2/lipid), which have been reported as a reasonable density range for pulmonary surfactant function from previous theoretical studies.[50−52] All four surface densities exhibit similar characteristic behavior (Figure S2 in the Supporting Information). We then performed 2.0 ns duration MD simulations of the POG/SP-B_{1-25}/water monolayer with 60 Å^2/lipid surface density as a representative case. The final snapshot in Figure 8a shows that the SP-B_{1-25} is located at the air−liquid interface. The hydrophobicity index of each AA residue in the peptide is shown in the top panel of Figure 8b.[53] Relatively strong hydrophobicity is found for the N-terminal side of the peptide, which contains Leu, Ile, and Pro residues. In contrast, hydrophilicity is expected from the C-terminal side as a result of the Arg, Lys, and Gln residues. The MD-simulated $\Delta z_{C\alpha}$ exhibits a good correlation with the hydrophobicity index. The hydrophobic N-terminal side of the peptide is located above the air−liquid interface ($\Delta z \approx 0$), while the hydrophilic C-terminal side is located inside or at the interface (Figure 8b bottom). Figure 8c shows the atomic density profiles of the oxygen atoms of water molecules as well as saturated and unsaturated carbon atoms of POG acyl chains along Δz. The 100-times-scaled atomic density profiles of the C_α carbons of the Cys_8, Trp_9, Cys_{11}, and Met_{21} residues are also shown in Figure 8c. The density profiles show a good agreement with the hydrophobicity index. In practice, a low water density is found around Trp_9, which is consistent with the formation of NFKyn via direct ozonolysis. The water density around Met_{21} is observed to be sufficiently high to expect secondary ROS formation and subsequent reaction to yield MetSO. In contrast, the low water density near Cys_8 and Cys_{11} inhibits formation of secondary ROS that would lead to their oxidation.

On the basis of the competitive reactivity of POG and SP-B_{1-25} with O_3, we suggested above that they are colocated at the interface. The MD simulations of SP-B_{1-25} in a lipid monolayer support our interpretation. Trp_9 and Met_{21} of SP-B_{1-25} lie below (in the z direction) the location of the lipid double bonds (Figure 8c). Figure 9a shows the xy-projected density profiles of the alkyl groups of the lipids with the averaged positions of the C_α carbons of the AA residues of

(50) Kaznessis, Y. N.; Kim, S.; Larson, R. G. *J. Mol. Biol.* **2002**, *322*, 569–582.
(51) Baoukina, S.; Monticelli, L.; Risselada, H. J.; Marrink, S. J.; Tieleman, D. P. *Proc. Natl. Acad. Sci. U.S.A.* **2008**, *105*, 10803–10808.
(52) Kaznessis, Y. N.; Kim, S. T.; Larson, R. G. *Biophys. J.* **2002**, *82*, 1731–1742.
(53) Kawashima, S.; Ogata, H.; Kanehisa, M. *Nucleic Acids Res.* **1999**, *27*, 368–369.

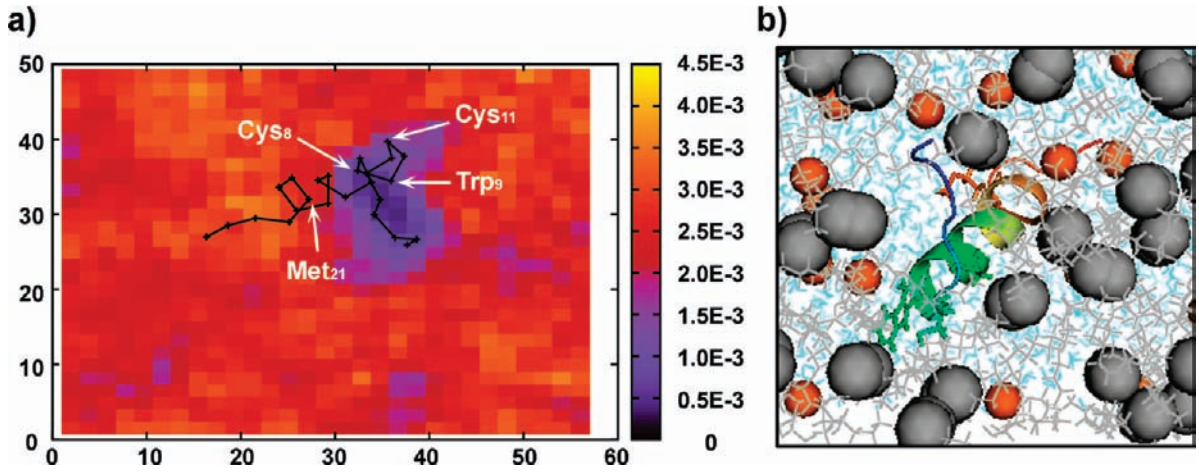

Figure 9. (a) The *xy*-projected density profiles of saturated carbon atoms of lipid acyl chains from MD simulations are shown with colors and the averaged positions of the C_α carbons of SP-B_{1-25} in the POG monolayer are shown with a black line (each residue is shown with cross). (b) Top view of the final snapshot after a 2.0 ns MD simulation of SP-B_{1-25} in a POG monolayer at 60 Å^2/lipid. The peptide is shown in rainbow color (C-terminal, red; N-terminal, blue). Lipids and water molecules are shown in gray and cyan, respectively. Black spheres denote unsaturated carbon atoms of lipid acyl chains, and orange spheres denote hydroxyl oxygen atoms.

SP-B_{1-25}. Consistent with our observation of the competitive interfacial reactivity of POG and SP-B_{1-25}, it is noteworthy that lipid acyl chains do not shelter the peptide at the air−liquid interface. The top view of the MD simulation final snapshot in Figure 9b illustrates that SP-B_{1-25} is not shielded by the unsaturated carbons (black spheres) of the lipids. The strong amphiphilic characteristic and the large surface area of SP-B_{1-25} cause the peptide to position itself at the air−liquid interface, where it displaces lipids. As a result, SP-B_{1-25} forms an island in a lipid monolayer that causes the hydrophobic portion of the peptide to be exposed to O_3 despite its location below the position of the lipid double bonds. We also simulated SP-B_{1-25} in the POPG monolayer, which is representative of the anionic unsaturated phospholipids in the PS.[54] The POPG monolayer exhibits atomic density profiles that are almost identical to those of the POG monolayer with 60 Å^2/lipid surface density (Figure S3 in the Supporting Information). A slightly stronger interaction between POPG and water is observed from their larger area of overlapping density (~1.6 times). This is due to the strong ion−dipole interactions between the POPG phosphate group and water molecules, which is absent from the POG monolayer. The peptide penetrates deeper into the POPG monolayer because of the strong electrostatic interaction between the cationic AA residues (Arg_{12}, Arg_{17}, and Lys_{16}) and the anionic phosphate group of POPG (Figure S4a,b in the Supporting Information), which agrees with previous simulations in anionic lipid monolayers.[50,55] SP-B_{1-25} forms an island in the POPG monolayer, and the anhydrous environment in the lipid monolayer renders SP-B_{1-25} more susceptible to direct ozonolysis than to modification by secondary ROS (Figures S4c and S5 in the Supporting Information).

Conclusions

In summary, to understand the unique chemistry of a surfactant protein at a model lung surfactant−air interface under O_3 exposure, we utilized the unique sampling capability of the FIDI-MS technique to examine chemical reactions in this boundary region. In the FIDI-MS spectra, oxidized products distinct from those formed in the solution phase were observed from SP-B_{1-25} alone and embedded in the POG monolayer. We also carried out MD simulations that provided additional insights into the interactions between lipids, SP-B_{1-25}, and water molecules in the interfacial region. In these simulations, the location of SP-B_{1-25} relative to the lipids provided a rationalization for the experimental observation that the peptide competes with the lipids for reaction with O_3.

Possible protection of SP-B from homogeneous oxidation by PS lipids has been suggested in an earlier study.[13] However, we have shown that SP-B_{1-25} is oxidized directly by heterogeneous reaction with O_3, as it is located at the air−liquid interface with significant exposure to O_3. The solution-phase oxidation of SP-B by secondary ROS is known to reduce its surface activity and function.[13,15] We have observed fast formation of NFKyn from the direct ozonolysis of Trp_9 on the hydrophobic N-terminal side of SP-B_{1-25}. Our data are consistent with a model in which the oxidized residue reduces the hydrophobicity of the N-terminal side of SP-B_{1-25}, facilitating migration of the peptide from the interfacial region to the liquid phase. This would result in NFKyn, Cys_8, and Cys_{11} being further oxidized by exposure to secondary ROS. In separate studies, we also examined the heterogeneous ozonolysis of a mixture of saturated and unsaturated phospholipids at the air−liquid interface using FIDI-MS. Only the unsaturated lipid reacts with ozone, forming products that are more water-soluble. With extensive ozonolysis, only the saturated lipid remains at the droplet surface.[56]

Our findings present a detailed explanation for the mechanisms of the possible damage to the pulmonary surfactant protein SP-B by secondary ROS or direct ozone exposure. Further studies with a more elaborate model system comprising SP-B, SP-C, and various lipids could further clarify the

(54) Yu, S.; Harding, P. G. R.; Smith, N.; Possmayer, F. *Lipids* **1983**, *18*, 522–529.
(55) Freites, J. A.; Choi, Y.; Tobias, D. J. *Biophys. J.* **2003**, *84*, 2169–2180.
(56) Kim, H. Ph.D. Thesis, California Institute of Technology, Pasadena, CA, 2009.

effect of other environmental exposures, such as smoking and airborne particles, on our lung surfactant system.

Acknowledgment. The research described in this paper was carried out at the Beckman Institute and the Noyes Laboratory of Chemical Physics at the California Institute of Technology, the Computational NanoBio Technology Laboratory at Georgia Institute of Technology, and the Jet Propulsion Laboratory under a contract with the National Aeronautics and Space Administration and funded through the Director's Research and Development Fund. We gratefully acknowledge financial support provided by National Science Foundation (NSF) under Grant CHE-0416381 (J.L.B., PI) and the Beckman Institute Mass Spectrometry Resource Center. Y.S.S. and J.R.H. acknowledge the support of the National Cancer Institute under Grant 5U54 CA119347 (J.R.H., PI).

Supporting Information Available: Additional figures and complete ref 35. This material is available free of charge via the Internet at http://pubs.acs.org.

JA908477W